Three-part differential of unlabeled leukocytes with a compact lens-free imaging flow cytometer

Supplementary Information

Dries Vercruysse,[1,2,*] Alexandra Dusa,[1] Richard Stahl,[1] Geert Vanmeerbeeck,[1] Koen de Wijs,[1,2] Chengxun Liu,[1] Dimiter Prodanov,[1] Peter Peumans,[1] and Liesbet Lagae[1,2]

[1]IMEC, Kapeldreef 75, B-3001 Leuven, Belgium
[2]INPAC and Dept. of Physics, KU Leuven, Celestijnenlaan 200 D, B-3001 Leuven, Belgium

---

*Electronic address: Dries.Vercruysse@imec.be
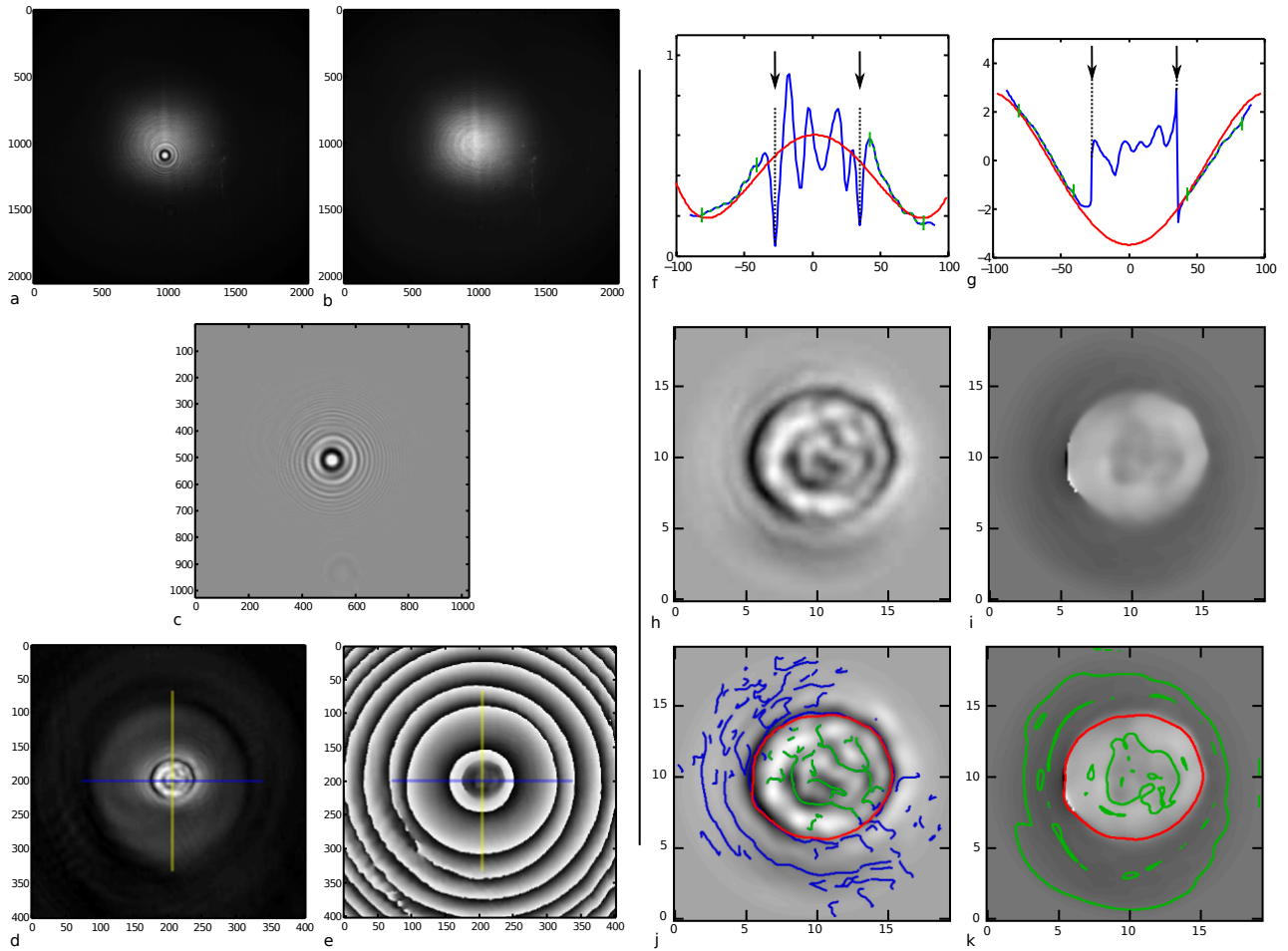
Reconstruction and virtual image removal

FIGURE S 1: Hologram analysis: (a) hologram of in-flow cell, (b) background, (c) cropped normalized hologram with background subtraction, (d) amplitude of the reconstructed hologram, (e) phase of the reconstruction, (f) cross section of the amplitude(blue) and the estimated fit of the virtual image(red) based on the green curves, (g) cross section of the phase and the estimated fit of the virtual image, (h) amplitude image with virtual image subtraction, (i) phase with virtual image subtraction, (j) amplitude image with detected ridges and the cell edge in red, (k) phase image with detected edges.

Figure S1a depicts a raw hologram taken with the high speed camera of a cell flowing under the pinhole. Figure S1b is captured under the same conditions, but as it does not contain a cell, it consequently serves as background. Note that a faint vertical line runs through the both images. This corresponds to the laminar flow generated by the central hydrodynamic focusing channel which delivers the blood cells, and is triggered by a small difference between the refractive index of sample-containing medium and the focusing medium. All cells follow this line, as is depicted in Figure S1a. Prior to reconstruction, the background is subtracted and the image is normalized. The normalization is done by dividing the background-subtracted image by the value of the background at the maximum of the hologram. The normalized image is subsequently cropped around the central maxima of the fringe pattern to form a 1024 by 1024 pixel image, as shown in Figure S1c. The hologram is then diffracted back to the channel plane by using the spectral algorithm approach:

$$U = \mathscr{F}^{-1}\{\mathscr{F}\{H\} \cdot e^{\frac{i2\pi d}{\lambda}\sqrt{1-m^2-n^2}}\} \tag{1}$$

with H, the captured hologram, d, the reconstruction depth and m and n the spatial frequencies. The reconstruction depth for this geometry is a combination of the distance from the camera to the pinhole, Zcc, and the distance from

the camera to the sample, Zco,:[1]

$$d = \left(\frac{1}{Z_{cc}} - \frac{1}{Z_{pc}} \right)^{-1} \tag{2}$$

The amplitude and phase of the reconstruction are shown in Figures S1d and S1e. The cell is clearly detectable in both images although the concomitant presence of the virtual image diminishes their clarity. This extra fringe pattern can be observed in the background of the amplitude image (Figure S1d) and in the background of Figure S1e as a phase well. There are multiple methods describing virtual image removal, but they often require multiple reconstruction steps moving back and forth between the hologram, image and virtual image plane, which tends to slow down the reconstruction algorithm. It should be noted that the virtual image is not a major concern when a single small object is being imaged, since in the absence of neighbouring objects no high frequency fringes will overlap with the object. This is almost always the case in our system, since there are no cells present in the focusing medium in the left and right channels, and since the cell concentration is low enough so that there is typically only one cell passing at a time. To roughly remove the virtual image, a 2D fourth order polynomial is fitted based on points outside the cell of the 2D cross-section as indicated in Figures S1d and S1e. This is done for the amplitude as well as the phase. Figures S1f and S1g depict the amplitude and phase on the blue cross-section. The dashed green lines represent the points used for the fit, and they lie outside the cell border indicated by the vertical dashed black line and arrows. The red curve is the fitted on a fourth order polynomial. The difference between the reconstruction and the fit for the amplitude and phase is shown in Figures S1h and S1g, respectively. Since the fit only applies to the region within the green boundaries, only this section shown in these images.

Starting from Figure S1h, the axes are labeled in micrometers. In order to correctly measure distances in the reconstruction, the system needs to be calibrated. Several images of the central microfluidic focusing channel are acquired at different pinhole heights. Based on the known width of this channel, the size of the pixel pitch in the reconstruction is linked to the reconstruction dept. A linear fit through these points is used to find the reconstruction pixel pitch once the reconstruction depth of the cell is known.

Finally, a scale space analysis is applied to locate the cell edge and estimate its internal complexity. In a scale-space analysis the analyzed image is typically smoothed by a Gaussian prior to applying a recognition operator. The standard deviation of the Gaussian is a measure of the smoothing and determines the size of the detected features in the image. It is therefore also called the scale parameter. The operator applied to find edges is the second local derivative. The zero-crossing of this derivative is considered an edge. Since we are only interested in the zero-crossings, this condition can be simplified to an expression which only contains partial derivatives in the xy-system:[2]

$$L_x^2 L_{xx} + 2L_x L_y L_{xy} + L_y^2 L_{yy} = 0 \tag{3}$$

with L_x and L_{xx}, the first and second partial derivative in the x-direction, with L_y L_{yy}, the first and second partial derivative in the y-direction, and with L_{xy}, the partial derivative in x- and y-direction. In order to find the cell edge this method is applied on the phase image. The detected edges can be visualized in green and red in Figure S1k. The scale parameter applied here is $5\mu m$, since the target structure, a cell, is large. The average intensity over each edge is subsequently calculated. The edge with a average diameter between 5 and 11 μm with the lowest value is labeled the cell edge. The diameter of a circle fitted through this edge is the cell diameter. For the internal complexity, the ridges inside the cell edge need to be detected. A ridge is defined as a zero-crossing in a first-order local derivative. This condition can be formulated as follows:

$$\begin{cases} L_q = 0 \\ L_{qq} < 0 \\ L_{qq} \geq L_{pp} \end{cases} \tag{4}$$

with L_q and L_{qq}, the first and second local derivative in the local q-direction, with L_{pp} second local derivative in the p-direction and with the pq-system the local coordinate system as defined in ref 2. The ridges detected in the intensity images are depicted in green and blue in Figure S1j. The internal complexity is only evaluated inside the cell edge (green). Once identified, the internal complexity is evaluated by the contrast of the internal edges which is gauged by the average of the Laplacian on the edge.

Computation time

The presented analysis was performed with a series of MATLAB scripts, dividing the total analysis in 3 separate parts: checking an image for presence of a cell in its center, reconstructing the hologram, and a scale space analysis to measure cell size and internal complexity. This MATLAB implementation contains some redundancy, saving and plotting many of the intermediate results causing the analysis on a set of 12000 images to take over an hour. A short study of this algorithm was performed in order to evaluate the required analysis time to process one 12000 image set on an Intel(R) Core(TM) i7 920 at 2.67GHz (=quad core with HyperThreading). A concise version of the algorithm based on open source code from [3] and [4] was used for this exercise. In the table below the execution times as well as analysis frames per second (fps) are shown for each part.

TABLE S I: Computation time for

	execution time(ms)	fps	total execution time for 12000 images (min)
Cell check	42	24	8.3
Cell check(without load)	20	50	4.0
Reconstruction (for 14% cells)	52	19	1.4
Scale space analysis (for 14% cells)	20	50	0.56
Total (for 14% cells)	109	9.2	10
Total (for 14% cells)(without load)	87	11	6.0

For the first part, checking the images for, presence of cells, the values are given with and without taking the image load kernel into account. This is done since in a more integrated solution the images might immediately go to analysis hardware and avoid a file system. After the cell check, we assume that about 14% of the images contained a cell, which agrees with what was observed in the experiments. We subsequently ran the reconstruction and scale space analysis on this 14%. When summing up all the execution times, the 12000 images can be analysed in approximately 10 min or 5.9 min without accounting for the image load kernel. Most of this analysis time is taken up by the cell check, since it has to go through all the images, and the reconstructions, since it uses ffts on 1024x1024 images. The scale space analysis requires much less time because it is executed on a much smaller image, the 200x200 center of the reconstruction, where the cell is located.

Total experimental counts

TABLE S II: Total counts of the isolated WBCs; The first row shows the total amount of images taken. The second row shows how many images contained a cell and the third and forth row show how many of these cells could be analysed in total and in percentages, respectively. (Errors in the analysis are most often caused by unwrapping issues)

	Granulocytes	Lymphocytes	Monocytes
Images	16380	7076	11635
Cells	774	764	1202
Successful analysis	662	734	1151
Successful analysis(%)	85.5	96.1	95.8

TABLE S III: Total counts of the whole blood measurements for each test; The first row displas the number of images containing a cell. The second row shows how many of these cells were successfully analysed.

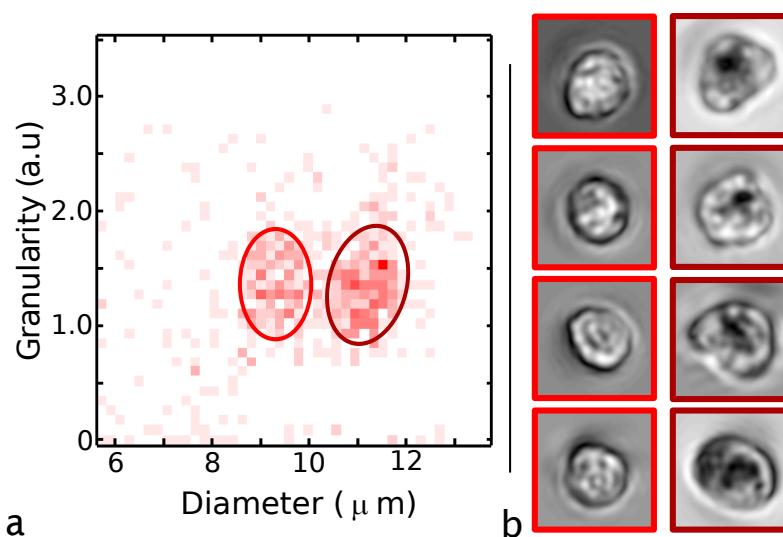|	Test1	Test2	Test3	Test4	Test5	Total
Cells	2023	1975	1890	1654	1093	8635
Successful analysis	1776	1695	1624	1434	954	7483

Purified cells activation

FIGURE S 2: Purified granulocytes: (a) 2D histogram of the diameter and granularity of purified granulocytes, (b) images of reconstructed cells in the left and right lobe indicated in panel a are shown in the left and right column, respectively.
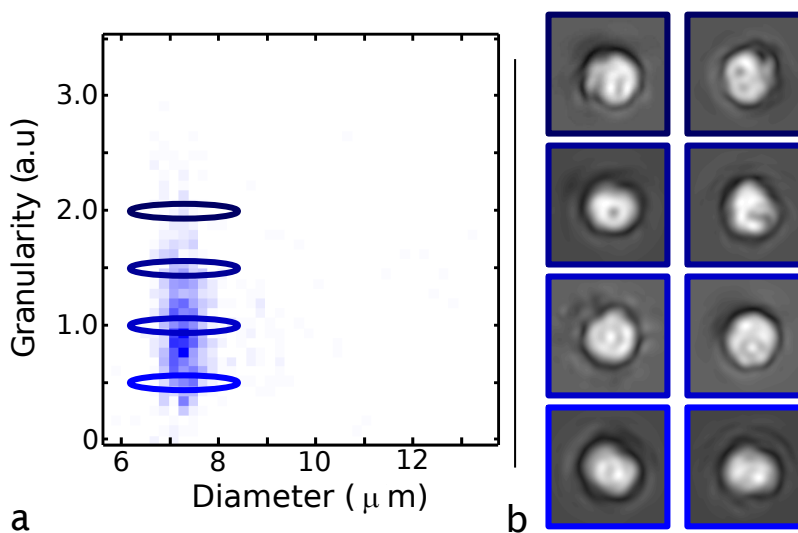

FIGURE S 3: Purified lymphocytes: (a) 2D histogram of the diameter and granularity of purified lymphocytes, (b) images of reconstructed cells with a granularity around 2, 1.5, 1 and 0.5 shown from top to bottom.
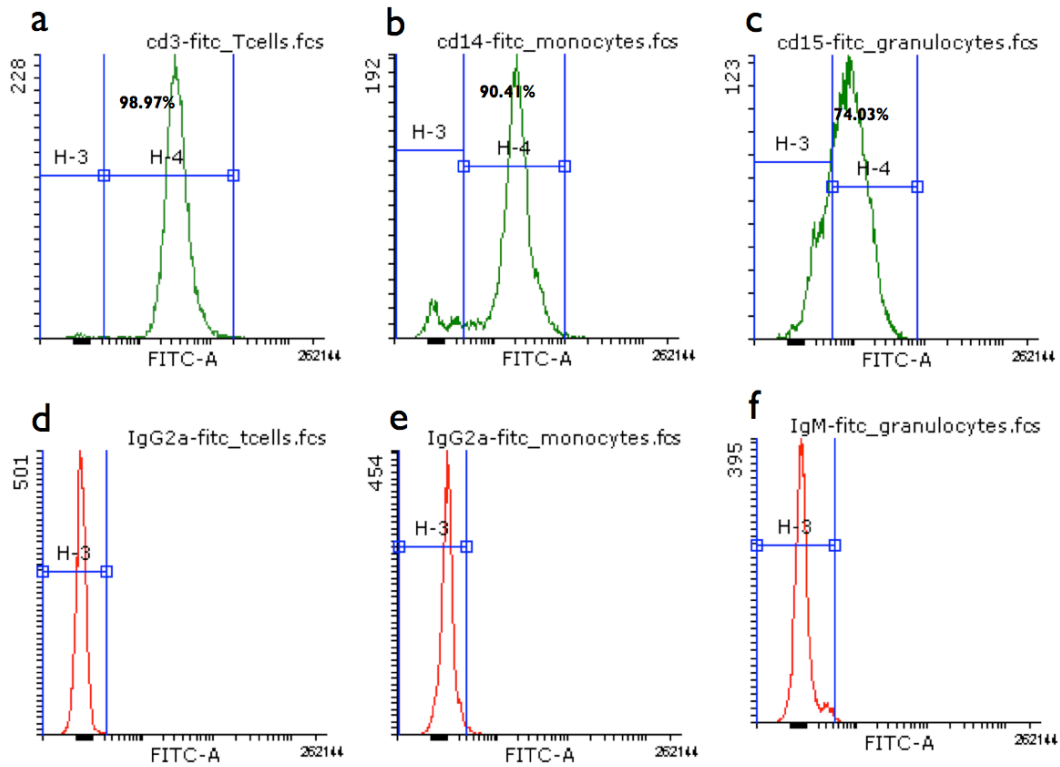
Purity assessment of purified blood populations by flow cytometry

FIGURE S 4: Histograms displaying fluorescence intensities of T-lymphocytes (a), monocytes (b) and granulocytes (c), fluorescently labeled with FITC-anti-CD3, FITC-anti-CD14 and FITC-anti-CD15 antibodies, respectively. The purity of each leukocyte fraction was assessed by taking into account the fluorescence signals generated by FITC-labeled isotype-matched control antibodies (d-f). The calculated purity values are in good agreement with previous reports.[5] The lower percentage of CD15-expressing granulocytes is due to the fact that for these cells, initial positive selection with CD-specific magnetic microbeads was deliberately avoided in order to keep inadvertent cell activation to a minimum.[6] The granulocyte fraction was instead purified by Polymorphprep density gradient centrifugation, which is not CD15-specific.

1. T. Kreis.*Handbook of Holographic Interferometry; Optical and Digital Methods*; John Wiley & Sons, 2006.

2. Lindeberg, T. *Edge detection and ridge detection with automatic scale selection*; International Journal of Computer Vision 1998, 30, 117156.

3. http://opencv.org.

4. http://www.fftw.org.

5. L. Zhou, R. Somasundaram, R. F. Nederhof, G. Dijkstra, K. N. Faber, M. P. Peppelenbosch and G. M. Fuhler, *Impact of Human Granulocyte and Monocyte Isolation Procedures on Functional Studies*; Clinical and Vaccine Immunology, 2012, 19, 1065-1074.

6. M. J. Cotter, K. E. Norman, P.G. Hellewell and V. C. Ridger, *A novel method for isolation of neutrophils from murine blood using negative immunomagnetic separation*; The American journal of pathology, 2001, 159, 473-481.